Electron-Pair Excitations and the Molecular Coulomb Continuum

J. M. Feagin,[1] J. Colgan,[2] A. Huetz,[3] and T. J. Reddish[4,*]

[1]*Department of Physics, California State University-Fullerton, Fullerton, California 92834, USA*
[2]*Theoretical Division, Los Alamos National Laboratory, Los Alamos, New Mexico 87545, USA*
[3]*CNRS, Université Paris-Sud, LIXAM UMR8624, Bâtiment 350, Orsay, Cedex, F-91405, France*
[4]*Department of Physics, University of Windsor, 401 Sunset Avenue, Ontario, Canada, N9B 3P4*

(Received 21 February 2009; published 15 July 2009)

Electron-pair excitations in the molecular hydrogen continuum are described by quantizing rotations of the momentum plane of the electron pair about the pair's relative momentum. A heliumlike description of the molecular photodouble ionization is thus extended to higher angular momenta of the electron pair. A simple three-state superposition is found to account surprisingly well for recent observations of non-coplanar electron-pair, molecular-axis angular distributions.

DOI: 10.1103/PhysRevLett.103.033002 PACS numbers: 33.80.Eh, 34.10.+x

One of the surprises of early observations of photodouble ionization of molecular hydrogen was the close similarity with the corresponding electron-pair angular distributions well established in helium, especially for relatively low-energy electron pairs [1]. The helium (free-atom) double ionization angular distributions, viz., the triple differential cross sections (TDCS), have a remarkably simple form for equal-energy ejected electrons, namely,

$$\text{TDCS} \sim |\hat{\epsilon}\cdot\mathbf{k}_1 + \hat{\epsilon}\cdot\mathbf{k}_2|^2 = |\hat{\epsilon}\cdot\mathbf{k}_+|^2, \qquad (1)$$

with $\hat{\epsilon}$ the photon polarization. Here $\hbar\mathbf{k}_+ = \hbar\mathbf{k}_1 + \hbar\mathbf{k}_2$ is the momentum of the photoejected electron-pair center of mass. The simplicity of this result derives from the underlying $^1S^e \to {}^1P^o$ dipole excitation. In molecular dipole excitation, the geometry of the molecule naturally resolves the photon polarization into components parallel (Σ) and perpendicular (Π) to the relative momentum direction $\mathbf{K}_- \equiv (\mathbf{K}_1 - \mathbf{K}_2)/2$ of the Coulomb-exploding ion pair [2], so that

$$\hat{\epsilon} \to \epsilon_\Pi + \epsilon_\Sigma = \sin\theta_N \hat{\epsilon}_\Pi + \cos\theta_N \hat{\mathbf{K}}_-, \qquad (2)$$

with $\cos\theta_N \equiv \hat{\epsilon}\cdot\hat{\mathbf{K}}_-$. Thus, with the heliumlike amplitude $\hat{\epsilon}\cdot\mathbf{k}_+$ from Eq. (1), one obtains an approximate molecular double ionization distribution or fully differential cross section (FDCS) for equal-energy ejected electrons according to

$$\text{FDCS} = |a_\Pi \sin\theta_N \hat{\epsilon}_\Pi\cdot\mathbf{k}_+ + a_\Sigma \cos\theta_N \hat{\mathbf{K}}_-\cdot\mathbf{k}_+|^2, \qquad (3)$$

where the a_Λ are undetermined dipole amplitudes internal to the molecule but independent of the momenta of the ionization fragments. This expression helps to explain the observed close similarity of low-energy helium and molecular hydrogen angular distributions. It is readily extended to unequal energy sharing and thus gives remarkably good fits to a variety of data, especially for coplanar geometries with respect to the ion- and electron-pair momenta and photon polarization.

Gisselbrecht *et al.* recently identified, however, equal-energy-sharing electron-pair configurations in the molecular fragmentation for which the heliumlike description categorically fails [3]. Their observations follow from earlier experiments by Weber *et al.* [4]. These anomalous angular distributions are noncoplanar and occur when one electron is observed perpendicular to the plane of the other and the polarization direction with the ion-pair direction $\mathbf{K}_-$ either parallel or perpendicular to the polarization. Gisselbrecht *et al.* termed these and related configurations *frozen correlation*, since the electron-pair angular separation $\hat{\mathbf{k}}_1\cdot\hat{\mathbf{k}}_2$ is held fixed in all three cases.

Parallel to these experimental achievements and insights, the community has seen decisive advancement in the *ab initio* computation of Coulomb few-body fragmentation, in particular, from two groups, one using a time-independent close-coupling approach with exterior complex scaling (ECS) [5] and one using a time-dependent close-coupling approach (TDCC) [6]. Their abundant "virtual data" are in excellent agreement in both magnitude and angular distribution with a wide variety of experimentally measured cross sections for both the coplanar and noncoplanar geometries. Results of the TDCC calculation [6] for these three distributions are shown in Fig. 1 and when folded over the experimental angular acceptances agree well with experiment (see the insets).

For each of these three configurations, one readily sees that Eq. (3) predicts the same simple $\mathbf{k}_2$ angular distribution of one electron, namely, $\text{FDCS} \sim (\hat{\epsilon}\cdot\hat{\mathbf{k}}_2)^2 \equiv \cos^2\theta_2$ with respect to a laboratory z_L axis along $\hat{\epsilon}$ and a y_L axis along $\mathbf{k}_1$ of the other electron held fixed perpendicular to the $\mathbf{k}_2$, $\hat{\epsilon}$ plane. Thus, although Fig. 1(a) with ion-pair direction $\mathbf{K}_-$ held fixed along $\mathbf{k}_1$ shows good agreement with the heliumlike $\cos^2\theta_2$ description, Figs. 1(b) and 1(c) show increasing deviations which become especially strong in Fig. 1(c) with $\mathbf{K}_-$ held fixed along $\hat{\epsilon}$.

One is thus lead to reconsider the heliumlike description of molecular fragmentation and the role of higher angular

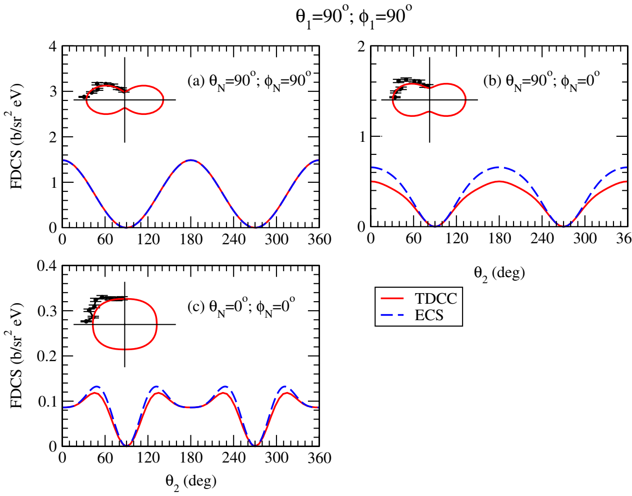

FIG. 1 (color online). H_2 photodouble ionization cross sections computed using time-dependent (TDCC) [6] and time-independent (ECS) [5] close coupling as a function of the orientation θ_2 of the momentum direction $\mathbf{k}_2$ of one electron relative to a laboratory z_L axis along the polarization direction $\hat{\epsilon}$ for 25 eV electron pairs with equal energy sharing. In each plot, the momentum direction $\mathbf{k}_1$ of the other electron is aligned along a y_L axis perpendicular to the $\mathbf{k}_2$, $\hat{\epsilon}$ plane. The three plots (a), (b), and (c) thus show three orientations θ_N, ϕ_N of the ion-pair direction $\mathbf{K}_-$ along the three axes y_L, x_L, and z_L, respectively. The polar-plot insets show a folded comparison with the experimental measurements of Gisselbrecht *et al.* [3].

momentum contributions to the electron pairs. In the molecular ground state, the electron-pair total angular momentum $\mathbf{L} = \boldsymbol{l}_1 + \boldsymbol{l}_2$ is not a good quantum number, so the heliumlike dipole selection rule ${}^1S^e \rightarrow {}^1P^o$ generalizes to ${}^1S^e, {}^1P^e, {}^1D^e, \ldots \rightarrow {}^1P^o, {}^1D^o, {}^1F^o, \ldots$ (the exchange and parity dipole selection rules remain the same).

Based on our longtime experience with electron-pair excitations in helium and H^-, it turns out to be advantageous—perhaps surprisingly so—to define states of total L by quantizing rotations of the momentum plane of the electron pair, depicted in Fig. 2, based on a z axis along their relative momentum direction $\mathbf{k}_- = (\mathbf{k}_1 - \mathbf{k}_2)/2$. One thus introduces symmetric-top wave functions $\tilde{D}^L_{Mm}(\hat{\mathbf{k}}_-)$ defined by projections $\hbar m = \mathbf{L} \cdot \hat{\mathbf{k}}_-$ and $\hbar M = \mathbf{L} \cdot \hat{\mathbf{z}}_M$, where $\hat{\mathbf{z}}_M$ is a molecular-frame z axis, which we will take here to be along the ion-pair relative momentum direction $\mathbf{K}_-$.

One thus constructs electron-pair momentum states of definite $LS\pi^e$ symmetry for $L \geq 1$ according to

$$\tilde{\psi}_M({}^{2S+1}L_\lambda) = \tilde{\phi}_\lambda(\mathbf{k}_+, k_-) \times [\tilde{D}^L_{M\lambda}(\hat{\mathbf{k}}_-) + \pi^e(-)^{L+\lambda}\tilde{D}^L_{M-\lambda}(\hat{\mathbf{k}}_-)], \quad (4)$$

where $\lambda \equiv |m|$. Here $\tilde{\phi}_\lambda(\mathbf{k}_+, k_-)$ is an internal state of the electron pair that describes only the relative orientation of the pair within the rotating $\mathbf{k}_1$, $\mathbf{k}_2$ plane and thus depends on $\mathbf{k}_+$, viz., k_{+x} and $k_{+z} \equiv \mathbf{k}_+ \cdot \hat{\mathbf{k}}_-$, and the magnitude $k_- = |\mathbf{k}_-|$ only.

In the case of dipole-allowed molecular fragmentation with linearly polarized photons in the axial-recoil approximation [2], we have the selection rules ${}^1\Sigma_g^+ \rightarrow {}^1\Lambda_u^+$, with $\Lambda \equiv |M| = 0, 1$ only, and therefore to consider just the two sets of states ${}^1\Sigma_u^+$ and ${}^1\Pi_u^+$ for any given L. We thus require the electron-pair states in Eq. (4) all to have ungerade (u) molecular symmetry and therefore $\pi^e =$ odd. We also require an additional even (+) symmetry with respect to reflections at any plane through $\mathbf{K}_-$ [7]. We find that the states in Eq. (4) reflect according to $\tilde{\psi}_M \rightarrow \pi^e(-)^{L+M}\tilde{\psi}_{-M}$. Thus, the dipole-allowed $\Lambda \equiv |M| = 0$ ${}^1\Sigma_u^+$ states have $L =$ odd only. In particular, the ${}^1\Sigma_u^+$ states with $L =$ even are dipole forbidden. For $\Lambda > 0$, we introduce the usual "Λ-doublet" linear combination

$$\tilde{\psi}_{\Lambda^+} = \frac{1}{\sqrt{2}}[\tilde{\psi}_\Lambda + \pi^e(-)^{L+\Lambda}\tilde{\psi}_{-\Lambda}], \quad (5)$$

which has even reflection symmetry for all L.

Although the analytic form of the internal wave function remains unknown (the few-body Coulomb problem remains unsolved), the decomposition of electron-pair states into symmetric-top wave functions has been used with good success to interpret and correlate a variety of observed dynamical symmetries and propensity rules in the doubly excited spectrum of helium and H^- both above and below the double ionization threshold [8].

For example, one can show quite generally [9] that the internal states have an inversion symmetry and therefore nodes as a function of $k_{+z} = \mathbf{k}_+ \cdot \hat{\mathbf{k}}_-$, viz., $\tilde{\phi}_\lambda(-k_{+z}) = \pi^e(-)^{S+\lambda}\tilde{\phi}_\lambda(k_{+z})$, so that in the case of equal energy sharing of interest here with $\mathbf{k}_+ \cdot \mathbf{k}_- = E_1 - E_2 = 0$, the dipole-allowed (singlet, $\pi^e =$ odd) internal states

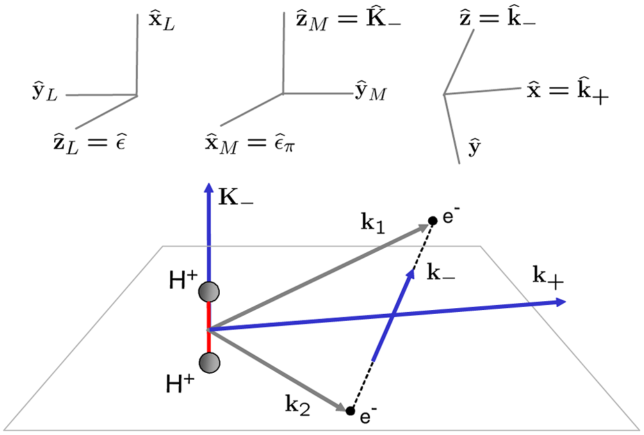

FIG. 2 (color online). Rotating $\mathbf{k}_1$, $\mathbf{k}_2$ plane of an ejected electron pair following the photofragmentation of molecular hydrogen. Here $\mathbf{k}_+ = \mathbf{k}_1 + \mathbf{k}_2$ and $\mathbf{k}_- = (\mathbf{k}_1 - \mathbf{k}_2)/2$ refer to the electron pair and $\mathbf{K}_- = (\mathbf{K}_1 - \mathbf{K}_2)/2$ to the ion pair. The top three insets illustrate the three frames of reference used in the text. Left to right: Laboratory, molecular, and electron-pair.

with $\lambda = \text{even}$ vanish identically, i.e., $\tilde{\phi}_{\lambda=\text{even}}(E_1 = E_2) \equiv 0$, for a given $L \geq \lambda$. For unequal energy sharing, these states will be weakly populated, and we have an example of a propensity rule.

We are now in a position to generalize to $L > 1$ electron pairs the heliumlike description of molecular fragmentation embodied in Eq. (3) by combining allowed ${}^1\Sigma_u^+$ and ${}^1\Pi_u^+$ states. We thus define dipole-allowed momentum states of an electron pair ejected into the molecular continuum according to

$$\tilde{\psi} = \sum_{L\geq 1}\sum_{\lambda\leq L} a_{L\Pi\lambda}\sin\theta_N \tilde{\psi}_{\Pi^+}({}^1L_\lambda) + a_{2L-1,\Sigma\lambda}\cos\theta_N \tilde{\psi}_{\Sigma^+}({}^1[2L-1]_\lambda), \tag{6}$$

where the $a_{L\Lambda\lambda}$ are undetermined dipole amplitudes describing the internal molecular excitation dynamics but independent of the momenta of the ionization fragments. Here, without loss of generality, we have taken the polarization $\hat{\boldsymbol{\epsilon}}$ to lie in the molecular $\hat{\mathbf{x}}_M$, $\hat{\mathbf{z}}_M$ plane, so that $\cos\theta_N = \hat{\mathbf{K}}_- \cdot \hat{\boldsymbol{\epsilon}}$ as before.

To connect our expansion Eq. (6) with Eq. (3), it is convenient to express the symmetric-top wave functions $\tilde{D}^L_{\Lambda\lambda}(\hat{\mathbf{k}}_-)$ in an angle-independent fashion in terms of the direction cosines $\hat{\mathbf{x}}_M \cdot \hat{\mathbf{x}}$, $\hat{\mathbf{y}}_M \cdot \hat{\mathbf{y}}$, $\hat{\mathbf{z}}_M \cdot \hat{\mathbf{z}}$, etc., connecting the molecular and the electron-pair frames. Along with a z axis along $\mathbf{k}_-$, it is convenient here for equal energy sharing $\mathbf{k}_+ \cdot \mathbf{k}_- = 0$ to take the electron-pair-frame x axis along $\mathbf{k}_+$ and thus the y axis along $\mathbf{k}_- \times \mathbf{k}_+ = \mathbf{k}_1 \times \mathbf{k}_2$ (see Fig. 2). We keep the molecular-frame z_M axis along $\mathbf{K}_-$ with $\hat{\mathbf{z}}_M = \hat{\mathbf{K}}_- = \hat{\boldsymbol{\epsilon}}_\Sigma$ and take $\hat{\mathbf{x}}_M = \hat{\boldsymbol{\epsilon}}_\Pi$ [cf. Eq. (2)], so that $\hat{\mathbf{y}}_M = \hat{\mathbf{K}}_- \times \hat{\boldsymbol{\epsilon}}_\Pi$.

With the frame axes thus defined in terms of the momentum vectors, we obtain the first three L contributions to Eq. (6) in a form analogous to Eq. (3) describing the dipole-allowed molecular states of the equal-energy electron-pair continuum according to

$$\begin{aligned}
\tilde{\psi}({}^1P_1) &\sim a_{1\Pi 1}\sin\theta_N \hat{\boldsymbol{\epsilon}}_\Pi \cdot \mathbf{k}_+ + a_{1\Sigma 1}\cos\theta_N \hat{\mathbf{K}}_- \cdot \mathbf{k}_+,\\
\tilde{\psi}({}^1D_1) &\sim a_{2\Pi 1}\sin\theta_N (\hat{\boldsymbol{\epsilon}}_\Pi \cdot \mathbf{k}_+ - 2\hat{\mathbf{K}}_- \cdot \hat{\mathbf{k}}_- \hat{\mathbf{y}}_M \cdot \hat{\mathbf{k}}_- \times \mathbf{k}_+),\\
\tilde{\psi}({}^1F_1) &\sim a_{3\Pi 1}\sin\theta_N \{[15(\hat{\mathbf{K}}_- \cdot \hat{\mathbf{k}}_-)^2 - 1]\hat{\boldsymbol{\epsilon}}_\Pi \cdot \mathbf{k}_+\\
&\quad - 10\hat{\mathbf{K}}_- \cdot \hat{\mathbf{k}}_- \hat{\mathbf{y}}_M \cdot \hat{\mathbf{k}}_- \times \mathbf{k}_+\}\\
&\quad + a_{3\Sigma 1}\cos\theta_N [1 - 5(\hat{\mathbf{K}}_- \cdot \hat{\mathbf{k}}_-)^2]\hat{\mathbf{K}}_- \cdot \mathbf{k}_+,
\end{aligned} \tag{7}$$

where we have dropped miscellaneous normalization constants. We have also introduced the analytic (Wannier) threshold limit $E_1 = E_2 = E/2 \rightarrow 0$ [9] for the internal wave functions $\tilde{\phi}_{\lambda=\text{odd}} \sim k_+^\lambda \sim E^{\lambda/2}$, which suggests the ${}^1F_{\lambda=1}$ state is favored in the low-energy spectrum over the allowed ${}^1F_{\lambda=3}$ mode, which will be presented elsewhere. Recall that the ${}^1P_{\lambda=0}$ as well as the ${}^1D_{\lambda=0,2}$ contributions are internal-inversion forbidden for equal energy sharing.

These results are readily applied to the frozen-correlation (fixed $\hat{\mathbf{k}}_1 \cdot \hat{\mathbf{k}}_2$) configurations of Fig. 1 defined relative to a laboratory z_L axis along the polarization direction $\hat{\boldsymbol{\epsilon}}$ and a y_L axis along the momentum direction $\mathbf{k}_1$ of one electron held fixed perpendicular to the $\mathbf{k}_2$, $\hat{\boldsymbol{\epsilon}}$ plane of the other. Superposing the three states in Eq. (7) thus gives the generalization of the molecular fragmentation distribution Eq. (3) according to

$$\text{FDCS} = N\cos^2\theta_2 |1 + B(\theta_N, \phi_N)\sin^2\theta_2|^2, \tag{8}$$

with $\cos\theta_2 = \hat{\boldsymbol{\epsilon}} \cdot \hat{\mathbf{k}}_2$. Here N is a normalization constant, while $B(\theta_N, \phi_N)$ is a ratio involving the various amplitudes $a_{L\leq 3,\Lambda 1}$ but independent of θ_2.

For the configuration in Fig. 1(a) with $\mathbf{K}_-$ held fixed parallel to $\mathbf{k}_1$ along the y_L axis, we thus find in fact that $B \equiv 0$, so that Eq. (8) reduces to the pure $\cos^2\theta_2$ dependence observed [10]. For the configurations in Fig. 1(b) with $\hat{\mathbf{K}}_- = \hat{\mathbf{x}}_L$ and in Fig. 1(c) with $\hat{\mathbf{K}}_- = \hat{\mathbf{z}}_L = \hat{\boldsymbol{\epsilon}}$, we find that $B \propto a_{3\Pi 1}$ and $B \propto a_{3\Sigma 1}$, respectively, giving the additional $\sin^2\theta_2$ dependence in Eq. (8). In Fig. 1(c), for the pure ${}^1\Sigma_g^+ \rightarrow {}^1\Sigma_u^+$ transition, there is no ${}^1D_{\lambda=1}$ contribution [11]. We have thus fitted Eq. (8) to the TDCC calculations, and Fig. 3 demonstrates that our rather simple three-state superposition captures surprisingly well the experimentally observed and *ab initio* close-coupling results from Fig. 1 [12].

The appearance of the axial vector $\mathbf{k}_- \times \mathbf{k}_+ = \mathbf{k}_1 \times \mathbf{k}_2$ and the resulting pseudoscalar $\hat{\mathbf{y}}_M \cdot \hat{\mathbf{k}}_- \times \mathbf{k}_+$ in the description of the molecular state Eq. (7) is a new feature of the $L > 1$ electron-pair continuum that is not observed in atoms. This special class of molecular fragmentation distributions was recently predicted in general terms [13]. Thus, it would be of interest to try to isolate the axial-vector contributions $\mathbf{k}_- \times \mathbf{k}_+$ experimentally. Inspection of Eq. (7) shows that these arise in the Π excitation only and could therefore be extracted by fixing $\mathbf{K}_- \perp \hat{\boldsymbol{\epsilon}}$, so that $\cos\theta_N = 0$, while selecting electron pairs with $\mathbf{k}_+ \perp \hat{\boldsymbol{\epsilon}}$. From Eq. (7), one then obtains $\tilde{\psi}({}^1P_1 + {}^1D_1 + {}^1F_1) \sim \hat{\mathbf{K}}_- \cdot \hat{\mathbf{k}}_- \hat{\mathbf{y}}_M \cdot \hat{\mathbf{k}}_- \times \mathbf{k}_+$, as desired. To fix $\mathbf{k}_+ \perp \hat{\boldsymbol{\epsilon}}$, one might start with the configuration in Fig. 1(b) with the z_L axis along $\hat{\boldsymbol{\epsilon}}$ and the x_L axis along $\hat{\mathbf{K}}_-$ (so that $\hat{\mathbf{y}}_L = -\hat{\mathbf{y}}_M$) and as depicted in Fig. 4 drop $\mathbf{k}_1$ in the y_L, $\hat{\boldsymbol{\epsilon}}$ plane behind

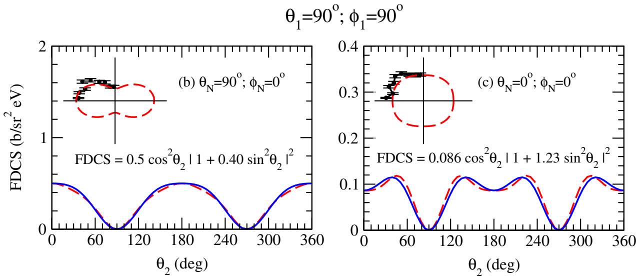

FIG. 3 (color online). Fits (solid curves) using Eq. (8) and thus a three-state superposition ${}^1P_{\lambda=1} + {}^1D_{\lambda=1} + {}^1F_{\lambda=1}$ from Eq. (7) to the H_2 photodouble ionization cross sections in Figs. 1(b) and 1(c). The dashed curves show the TDCC result from Fig. 1.

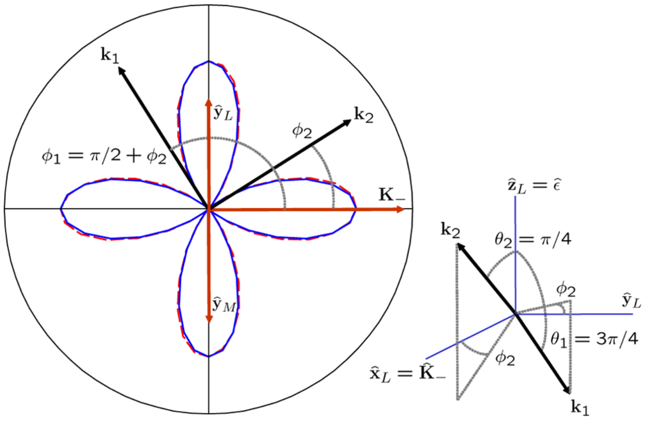

FIG. 4 (color online). An electron-pair angular distribution for fixed $\hat{\mathbf{k}}_1 \cdot \hat{\mathbf{k}}_2$ looking down a z_L axis along $\hat{\epsilon}$ onto the $\hat{\mathbf{x}}_L = \hat{\mathbf{K}}_-$, $\hat{\mathbf{y}}_L$ plane as a function of the azimuthal orientation ϕ_2 of the pair. Here $\mathbf{k}_2$ and $\mathbf{k}_1$ are oriented above and below, respectively, the $\hat{\mathbf{K}}_-$, $\hat{\mathbf{y}}_L$ plane (cf. 3D inset) with fixed polar angles $\theta_2 = \pi/4$ and $\theta_1 = \pi - \theta_2$ while varying ϕ_2 along with $\phi_1 = \phi_2 + \pi/2$. The solid four-lobe curve is the resulting $\cos^2 2\phi_2$ distribution predicted from the axial-vector contributions to Eq. (7), arbitrarily scaled to a TDCC calculation shown with the dashed curve. The circle radius equals 0.03 b/sr^2 eV.

$\mathbf{k}_2$ in the $\hat{\mathbf{K}}_-$, $\hat{\epsilon}$ plane taking $\theta_1 = \pi - \theta_2$. To maintain a frozen-correlation configuration, one can then sweep the electron pair azimuthally about $\hat{\epsilon}$ keeping $\hat{\mathbf{k}}_1 \cdot \hat{\mathbf{k}}_2$ fixed by varying the azimuthal angles ϕ_1, ϕ_2 of $\mathbf{k}_1$, $\mathbf{k}_2$ together with $\phi_1 = \phi_2 + \pi/2$. One then obtains the angular dependence $\hat{\mathbf{K}}_- \cdot \hat{\mathbf{k}}_- \hat{\mathbf{y}}_M \cdot \hat{\mathbf{k}}_- \times \mathbf{k}_+ \sim \cos\theta_2 \sin^2\theta_2 \cos 2\phi_2$ and thus a unique four-lobe angular distribution as a function of ϕ_2 [14].

In Fig. 4, we present evidence for this special configuration in the molecular fragmentation cross section calculated with the TDCC theory. One thus finds good agreement with the predicted cross section FDCS $\sim \cos^2 2\phi_2$ from the axial-vector contributions to Eq. (7). Besides being relatively weak, we find the distribution to be sensitive to folding over experimental angular acceptances (compare with the insets in Figs. 1 and 3), which quickly mixes back in the competing $\hat{\epsilon}_\Pi \cdot \mathbf{k}_+$ and $\hat{\mathbf{K}}_- \cdot \mathbf{k}_+$ distributions from Eq. (7) and tends to wash out the four-lobe structure.

Our molecular fragmentation description embodied in Eq. (6) might also be viewed as a judicious resummation of the expansions of the transition amplitudes used in the close-coupling approaches [5,6] based on pairs of one-electron harmonics $Y_{l_1 m_1}(\hat{\mathbf{k}}_1) Y_{l_2 m_2}(\hat{\mathbf{k}}_2)$ [15]. The frozen-correlation configurations we have examined here with fixed $\hat{\mathbf{k}}_1 \cdot \hat{\mathbf{k}}_2$, especially out of the $\hat{\mathbf{K}}_-$, $\hat{\epsilon}$ plane, have proven to be a strong test of the convergence of these approaches. (Typically, ~100 channels are needed.) The usefulness of the electron-pair modes defined in Eq. (4) is in the compact description of the continuum spectrum they afford even for frozen-correlation configurations. The same modes should in principle describe any low-energy electron-pair continuum, once appropriately symmetrized. Different systems would require only different sets of mixing coefficients $a_{L\Lambda\lambda}$. One might hope to thus establish a robust tool for analyzing a variety of experimental data including modeling of electron pairs ejected from more complex molecules and even surfaces and solids, for which *ab initio* calculations may not exist for some time.

This project has been supported by the Chemical Sciences, Geosciences and Biosciences Division of the Office of Basic Energy Sciences, U.S. Department of Energy. The Los Alamos National Laboratory is operated by Los Alamos National Security, LLC for the National Nuclear Security Administration of the U.S. Department of Energy under Contract No. DE-AC5206NA25396.

---

[*] jfeagin@fullerton.edu

[1] T. J. Reddish and J. M. Feagin, J. Phys. B **32**, 2473 (1999); J. M. Feagin, J. Phys. B **31**, L729 (1998).
[2] We invoke here the usual axial-recoil approximation and make no distinction between the spatial orientation of the molecular axis $\hat{\mathbf{R}}_N$ and the postselected relative momentum direction $\hat{\mathbf{K}}_-$ of the Coulomb-exploding ion pair on the heels of the swift electron-pair photoejection.
[3] M. Gisselbrecht *et al.*, Phys. Rev. Lett. **96**, 153002 (2006).
[4] Th. Weber *et al.*, Nature (London) **431**, 437 (2004); **443**, 1014 (2006).
[5] W. Vanroose, F. Martin, T. N. Rescigno, and C. W. McCurdy, Phys. Rev. A **70**, 050703(R) (2004); Science **310**, 1787 (2005).
[6] J. Colgan, M. S. Pindzola, and F. Robicheaux, J. Phys. B **37**, L377 (2004); Phys. Rev. Lett. **98**, 153001 (2007).
[7] G. Herzberg, *Spectra of Diatomic Molecules* (Van Nostrand Reinhold, New York, 1950), 2nd ed., Chap. 5; R. N. Zare, *Angular Momentum* (Wiley-Interscience, New York, 1988), Chap. 6.
[8] M. Walter, J. S. Briggs, and J. M. Feagin, J. Phys. B **33**, 2907 (2000).
[9] J. M. Feagin, J. Phys. B **29**, L551 (1996).
[10] This pure $\cos^2\theta_2$ dependence persists even if the ${}^1F_{\lambda=3}$ mode is included in the superposition.
[11] The ${}^1P_{\lambda=1}$ and ${}^1D_{\lambda=1}$ modes in Eq. (7) are degenerate and contribute simply $\hat{\epsilon}_\Pi \cdot \mathbf{k}_+$ in all three cases [Figs. 1(a)–1(c)].
[12] Although our approach gives little insight into the relative magnitudes of $a_{L\Pi\lambda}$ compared to $a_{L\Sigma\lambda}$ in Eqs. (6) and (7), Gisselbrecht *et al.* [3] determined their ratio in Eq. (3) to be 2.25 ± 0.35. Compare also the relative magnitudes of the cross sections shown in Figs. 1 and 3.
[13] M. Walter, A. V. Meremianin, and J. S. Briggs, J. Phys. B **36**, 4561 (2003).
[14] One also obtains a four-lobe distribution as a function of θ_2 for fixed ϕ_2, albeit one with non-frozen correlation.
[15] An analogous resummation in bipolar harmonics was derived to study selection rules and isotope effects by M. Walter and J. S. Briggs, Phys. Rev. Lett. **85**, 1630 (2000).